Accurate Mobile Robot Dead-reckoning With a Precision-calibrated Fiber Optic Gyroscope[1]

By

Hakyoung Chung[*], Lauro Ojeda[**], and Johann Borenstein[**]

[*] Seoul National University of Technology, Department of Control and Instrumentation Engineering, 172 Kongneung-dong, Nowon-gu, Seoul 139-743, Korea, chy@duck.snut.ac.kr

[**] The University of Michigan, Department of Mechanical Engineering, Mobile Robotics Lab, 1101 Beal Ave., Ann Arbor, MI 48109-2110, USA. lojeda@umich.edu, johannb@umich.edu.

ABSTRACT

This paper describes two methods aimed at improving dead-reckoning accuracy with fiber optic gyroscopes (FOGs) in mobile robots. The first method is a precision calibration procedure for FOGs, which effectively reduces the ill-effects of non-linearity of the scale-factor and temperature dependency. The second method is the implementation of an indirect feedback Kalman filter that fuses the sensor data from the FOG with the odometry system of the mobile robot.

The paper also provides experimental results and compares the relative effectiveness of the two methods as implemented on a four-wheel drive/skid-steer Pioneer AT mobile robot.

Key words: *Mobile robot, dead-reckoning, fiber optic gyroscope, indirect feedback Kalman filter, odometry.*

1. INTRODUCTION

Until just a few years ago all but the highest-grade mechanical gyroscopes had large bias drift rates. However, this situation changed with the reduction in cost of commercially available fiber optic gyroscopes (FOGs). For example, the KVH E-Core RD2100 gyro [1,2], which was the model used in our experiments, costs about $2,000 and its drift rate is specified as (at most) $0.002°/s = 0.12°/min = 7.2°/hr$ (see Table I for specifications as published by the manufacturer). However, with the reduction of bias drift errors other measurement errors gain in relative significance. Most notable among these hitherto secondary error are (1) the *nonlinearity of the scale factor* and (2) the *susceptibility of the sensor to changes in ambient temperature*. These two errors can be reduced substantially by performing an individual calibration for each FOG [3].

When more than one sensor modality is used to measure one parameter, such as the relative orientation of a mobile robot, then the question arises how to fuse the readings from both sensor modalities. Barshan and Durrant-Whyte [4] proposed a direct Kalman filter that estimates the robot

---

position and attitude. Other researches [5, 6] utilize gyroscopes and encoders to obtain a close estimate of the robot position. However, these methods need fast computations due to the rapidly varying nature of the robot dynamics. In this paper we propose an indirect Kalman filter that estimates error states and does not require fast computation [7].

The calibration procedure for the FOG is described in Section 2, while the design of our Kalman filter is detailed in Section 3. The complete dead-reckoning system was implemented on a Pioneer AT four-wheel drive/skid-steer mobile platform, and experimental results are provided in Section 4.

2. GYROSCOPE CALIBRATION

One well known source of errors in gyroscopes is the static bias drift. In this paper we are not focusing on this (significant) error source because a trivial short-term calibration method is effective in dealing with this problem: Prior to each mobile robot mission (i.e., while the robot is standing still) the gyro output is sampled for, say, 5 – 10 seconds, and the readings are averaged. Then, once the robot is moving, this averaged static bias value is subtracted from all subsequent gyro readings. Because of the relatively low static bias drift in FOGs, mission durations on the order of 10 minutes are feasible before a new static bias drift value should be determined by repeating the above short-term calibration.

Once the static bias error is reduced in the above described way, two other sources of errors become dominant: 1) the non-linearity in the scale factor and 2) the gyro's susceptibility to changes in ambient temperature. This section briefly explains the mathematical model for these errors, while a more detailed treatment can be found in [3].

2.1 Non-linearity of the scale factor

The basic idea for measuring scale factor errors is to rotate the gyro at a varying but precisely controlled input rates, ω, while comparing the measurement output of the gyro, ω_g, to the known input rates. The difference between both values is the error introduced by the non-linearity in the scale factor, ε.

$$e = w_g - w \cdot \tag{1}$$

The same procedure has to be repeated at different speeds trying to cover the whole range of operation of the gyro. The resulting errors (see typical example for one FOG in Figure 1) can be approximated by a third-order polynomial

$$e(w_g) = a_0 + a_1 w_g + a_2 w_g^2 + a_3 w_g^3 \cdot \tag{2}$$

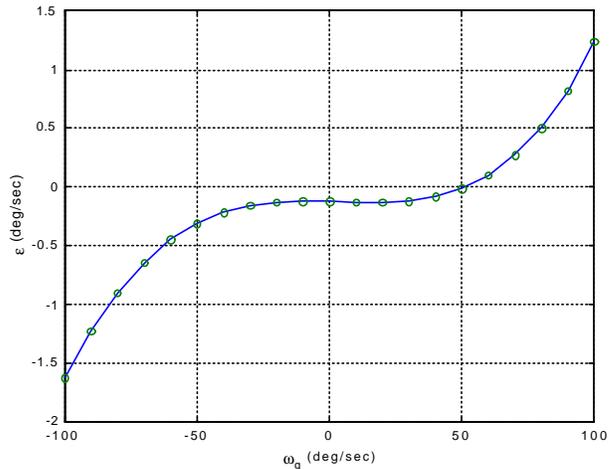**Figure 1:** The error due to the non-linearity in the scale factor. The range of input rates in this and all subsequent experiments was –100°/s to +100°/s.

2

2.2 Effect of the changes in temperature

Figure 2 shows how the measurement error ε varies with temperature. This relationship can be expressed in terms of a second-order polynomial

$$\boldsymbol{e}(t) = b_0 + b_1 T + b_2 T^2 . \tag{3}$$

Parameters b_i are not constant but depend of the input rate of rotation, ω. This means that all experiments must be repeated at different temperatures to calculate the final error model or compensation function of the gyro. The KVH E-core RD2100 FOG used in our experiments comes with a built-in temperature sensor and the readings from this sensor are available to the user within the data packets output by the FOG.
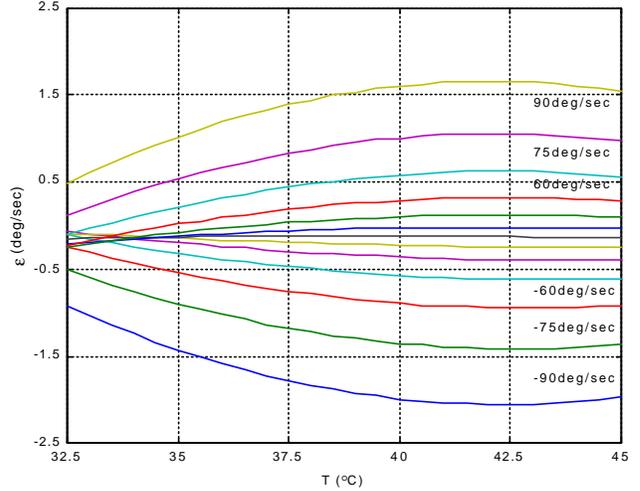

Figure 2: Gyro measurement errors due to changes in temperature at different rates of rotation.

2.3 Building the error function

This section discusses the mathematical formulation of the error function. We will refer to the gyro data collected during rotation at a fixed rate of rotation and at a fixed temperature as one *data set*. In practice this is done by defining two data vectors for each rate of rotation, $\boldsymbol{w}_i$. One for the output of the gyro, $\boldsymbol{w}_{gi}$, and the other for the corresponding temperatures, T_i, all of dimension n

$$\boldsymbol{w} = \begin{bmatrix} \boldsymbol{w}_1 \\ \boldsymbol{w}_2 \\ . \\ . \\ \boldsymbol{w}_n \end{bmatrix} \quad \boldsymbol{w}_g = \begin{bmatrix} \boldsymbol{w}_{g1} \\ \boldsymbol{w}_{g2} \\ . \\ . \\ \boldsymbol{w}_{gn} \end{bmatrix} \quad \mathbf{T} = \begin{bmatrix} T_1 \\ T_2 \\ . \\ . \\ T_n \end{bmatrix} \tag{4}$$

where n is the number of different rates of rotation multiplied by the number of temperature variations.

The difference between the output of the gyro, ω_{gi}, and the rate of rotation of the rotary table, ω_i, represents the error of the gyro ε_i at temperature T_i, (see Figure 3a).

The next step is to find a mathematical model of the error ε as a function of the known variables: the output of the gyro, ω_g, and the temperature, T

$$\boldsymbol{e} = f(T, \boldsymbol{w}_g) . \tag{5}$$

Table I: Technical specifications for the E-Core RD2100 fiber optic gyroscope. (Courtesy of [KVH])

Performance		RD2100
Input Rate (max)	± °/sec	100
Resolution	°/sec	0.004
Scale factor	°/bit	0.000305
Nonlinearity	%, rms	0.5
Full Temp	%, p-p	2
Bias Stability		
Constant Temp	°/sec	0.002
Full Temp	°/sec, p-p	0.2
Repeatability	°/sec, p-p	0.002
Angle Rand. Walk	(°/hr)/ Hz	5
	°/ hr	0.08
Bandwidth	Hz (for 3 dB with 45° phase shift)	100

Figure 3a shows experimental errors of one of the tested FOGs at different rates of rotation and temperatures without any compensation. Finding an error model from the measurements, ω_g and T, is a two-input single-output system identification problem. In order to use a general least-square algorithm, we adopted a *Vandermonde* matrix [8] that reduces the problem to a single-input single-output system. The thus fully defined error function $\varepsilon(\omega_g, T)$ can now be used as a compensation function, simply by subtracting the appropriate value of $\varepsilon(\omega_g, T)$ from every gyro measurement ω_g (see [3] for more details).

$$\boldsymbol{w}_g^* = \boldsymbol{w}_g - \boldsymbol{e}(\boldsymbol{w}_g, T) \tag{6}$$

where

ω_g - Gyro reading before compensation

ω_g^* - Compensated gyro reading

Figure 3b shows the errors of the FOG after correcting its output with the compensation function according to Eq. (6). Note that Figure 3b is the result of applying the compensation function to a completely new set of data (and not to the same set of data that was used to build the compensation function).

3. IMPLEMENTATION OF THE DEAD-RECKONING NAVIGATION SYSTEM
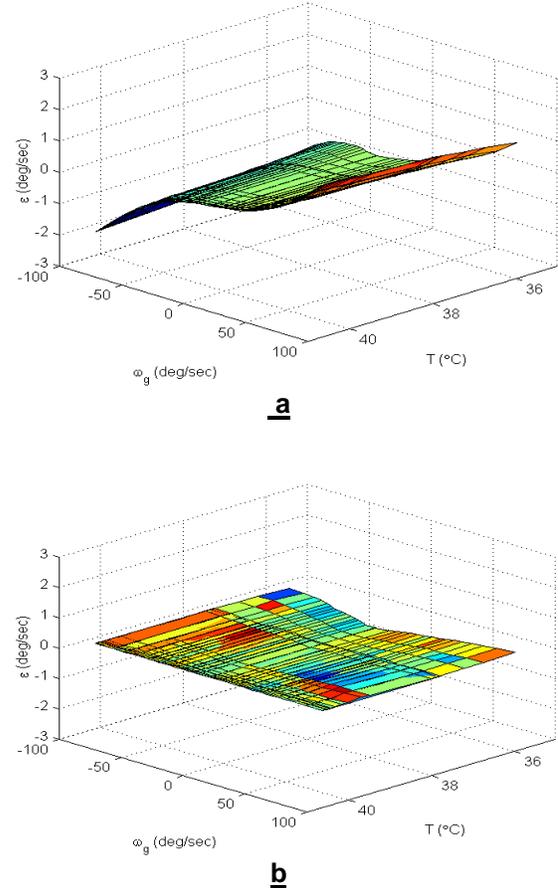

a

b

Figure 3: Experimental errors of the gyro at different speeds and temperatures.
(a) Without the compensation function
(b) After applying the compensation function.

One way of reducing position and orientation errors in dead-reckoning navigation systems is to meticulously model the sensor errors and design an appropriate filter accordingly. In this paper we implement an indirect Kalman filter that estimates error states and overcomes some of the disadvantages of conventional Kalman filters. The motivation for using this structure with differential drive mobile robots can be found in [9].

3.1 The error model for odometry

The mobile robot position and heading angle are calculated from the output of incremental encoders by

$$X(k+1) = X(k) + \sin \mathbf{y}(k) \times U(k)$$
$$Y(k+1) = Y(k) + \cos \mathbf{y}(k) \times U(k)$$
$$\mathbf{y}(k+1) = \mathbf{y}(k) + \frac{U_R(k) - U_L(k)}{D}$$
$$U(k) = \frac{U_R(k) + U_L(k)}{2}$$

(7)

where X and Y represent the mobile robot position in the navigation frame, and $\mathbf{y}$ is the heading of the mobile robot. U_R and U_L are the right and left wheel incremental distances respectively, and D is the tread distance between the left and right wheels.

It is well-known that odometry is subject to systematic errors caused by factors such as unequal wheel-diameters, imprecisely measured wheel diameters (i.e., the so-called scale-factor error), or an imprecisely measured tread (see [10] for a detailed discussion). Subject to these errors the robot's position and its heading angle are computed by

$$\hat{X}(k+1) = \hat{X}(k) + \sin \hat{\mathbf{y}}(k) \left(\frac{U_R + S_R(k)U_R + U_L + S_L(k)U_L}{2} \right)$$
$$\hat{Y}(k+1) = \hat{Y}(k) + \cos \hat{\mathbf{y}}(k) \left(\frac{U_R + S_R(k)U_R + U_L + S_L(k)U_L}{2} \right)$$
$$\hat{\mathbf{y}}(k+1) = \hat{\mathbf{y}}(k) + \frac{(U_R + S_R(k)U_R) - (U_L + S_L(k)U_L)}{D + \mathbf{d}D(k)}$$
$$\hat{X}(k) = X(k) + \mathbf{d}X(k)$$
$$\hat{Y}(k) = Y(k) + \mathbf{d}Y(k)$$
$$\hat{\mathbf{y}}(k) = \mathbf{y}(k) + \mathbf{d}\mathbf{y}(k)$$

(8)

where $\hat{X}(k), \hat{Y}(k)$, and $\hat{\mathbf{y}}(k)$ are the calculated position and heading angle. $X(k), Y(k)$, and $\mathbf{y}(k)$ are the true position and heading angle. $\mathbf{d}X(k), \mathbf{d}Y(k)$, and $\mathbf{d}\mathbf{y}(k)$ are the position and heading angle error. $\mathbf{d}D(k)$ is the tread error, i.e., the error introduced by variations in the distance between the left and right wheels. $S_R(k)$ and $S_L(k)$ are the scale factor errors of the right and left encoders, respectively.

Subtraction of the true position values from the calculated position values yields the error propagation equations

$$\mathbf{d}X(k+1) = \mathbf{d}X(k) + \sin \mathbf{y}(k) \frac{U_R}{2} S_R(k) + \sin \mathbf{y}(k) \frac{U_L}{2} S_L(k) + \cos \mathbf{y}(k) \frac{U_R + U_L}{2} \mathbf{d}\mathbf{y}(k)$$
$$\mathbf{d}Y(k+1) = \mathbf{d}Y(k) + \cos \mathbf{y}(k) \frac{U_R}{2} S_R(k) + \cos \mathbf{y}(k) \frac{U_L}{2} S_L(k) - \sin \mathbf{y}(k) \frac{U_R + U_L}{2} \mathbf{d}\mathbf{y}(k)$$
$$\mathbf{d}\mathbf{y}(k+1) = \mathbf{d}\mathbf{y}(k) + \frac{U_R}{D} S_R(k) - \frac{U_L}{D} S_L(k) + \frac{U_L - U_R}{D^2} \mathbf{d}D(k)$$

(9)

where we assumed that $\mathbf{d}\mathbf{y}(k)$ is small, i.e., $\cos \mathbf{d}\mathbf{y}(k) \cong 1$, $\sin \mathbf{d}\mathbf{y}(k) \cong \mathbf{d}\mathbf{y}(k)$, $\mathbf{d}\mathbf{y}(k)S_R(k) \cong 0$, $\mathbf{d}\mathbf{y}(k)S_L(k) \cong 0$, and $D(k) >> \mathbf{d}D(k)$. It is also assumed that there is no error in wheel alignment.

Left and right encoder scale factor errors and wheel separation distance errors are regarded as random constants due to their slow time-varying characteristics. Thus, these errors can be expressed by

$$S_R(k+1) = S_R(k)$$
$$S_L(k+1) = S_L(k)$$
$$\mathbf{d}D(k+1) = \mathbf{d}D(k).$$

(10)

For outdoor environments, zero-mean white Gaussian noise is added to (9) to represent ground irregularities, bumps, cracks, or slippage. These factors always add a positive error to the encoder reading, that is, the encoder will always add pulses but never miss pulses when encountering any such problem on the ground. In the error models, the random constants represent the average values of the irregular errors as well as the scale factor errors and tread error, while the white Gaussian noise represent small deviation of the average values of the irregular errors.

3.2 The error model for the gyroscope

The heading angle from a gyroscope with bias drift and scale factor error is represented by

$$
\begin{aligned}
\hat{f}(k+1) &= \hat{f}(k) + \hat{B}_s(k)\Omega + \hat{B}_{rb}(k) \\
\hat{B}_s(k) &= B_s + dB_s(k) \\
\hat{B}_{rb}(k) &= B_b(k) + dB_{rb}(k) \\
\hat{f}(k) &= f(k) + df(k)
\end{aligned}
\tag{11}
$$

where

$\hat{f}(k)$	-	calculated heading angle using the gyroscope
$f(k)$	-	true heading angle
Ω	-	angular rate [volt]
$\hat{B}_s(k)$	-	scale factor [°/sec/volt]
B_s	-	true scale factor
$\hat{B}_{rb}(k)$	-	gyroscope bias
$B_b(k)$	-	deterministic bias
$df(k)$	-	gyroscope heading angle error
$dB_s(k)$	-	gyroscope scale factor error
$dB_{rb}(k)$	-	gyroscope random bias error

A heading angle error equation for the gyroscope is obtained by subtracting $\hat{f}(k+1)$ from $f(k+1)$, as shown in Eq. (12). Bias and scale factor error can be modeled as random constants.

$$
\begin{aligned}
df(k+1) &= df(k) + \Omega dB_s(k) + dB_{rb}(k) \\
dB_s(k+1) &= dB_s(k) \\
dB_{rb}(k+1) &= dB_{rb}(k).
\end{aligned}
\tag{12}
$$

3.3 Implementation of the indirect Kalman filter

Using the linear error models, the resulting state equations of the indirect feedback Kalman filter, $\dot{x} = Ax + w$, are given by

$$
\begin{bmatrix}
dX(k+1) \\
dY(k+1) \\
dy(k+1) \\
S_R(k+1) \\
S_L(k+1) \\
dD(k+1) \\
df(k+1) \\
dB_s(k+1) \\
dB_{rb}(k+1)
\end{bmatrix}
=
\begin{bmatrix}
1 & 0 & \cos y(k)\dfrac{U_R+U_L}{2} & \sin y(k)\dfrac{U_R}{2} & \sin y(k)\dfrac{U_L}{2} & 0 & 0 & 0 & 0 \\
0 & 1 & -\sin y(k)\dfrac{U_R+U_L}{2} & \cos y(k)\dfrac{U_R}{2} & \cos y(k)\dfrac{U_L}{2} & 0 & 0 & 0 & 0 \\
0 & 0 & 1 & \dfrac{U_R}{D} & -\dfrac{U_L}{D} & \dfrac{U_L-U_R}{D^2} & 0 & 0 & 0 \\
0 & 0 & 0 & 1 & 0 & 0 & 0 & 0 & 0 \\
0 & 0 & 0 & 0 & 1 & 0 & 0 & 0 & 0 \\
0 & 0 & 0 & 0 & 0 & 1 & 0 & 0 & 0 \\
0 & 0 & 0 & 0 & 0 & 0 & 1 & \Omega & 1 \\
0 & 0 & 0 & 0 & 0 & 0 & 0 & 1 & 0 \\
0 & 0 & 0 & 0 & 0 & 0 & 0 & 0 & 1
\end{bmatrix}
\begin{bmatrix}
dX(k) \\
dY(k) \\
dy(k) \\
S_R(k) \\
S_L(k) \\
dD(k) \\
df(k) \\
dB_s(k) \\
dB_{rb}(k)
\end{bmatrix}
+w
\qquad (13)
$$

where ω is the process noise.

Measuring the difference between the heading angles computed by odometry and by the gyroscope, the measurement equation $Z = Hx + v$ is given by

$$
Z = \hat{y}(k) - \hat{f}(k) + v = dy(k) - df(k) + v = \begin{bmatrix} 0 & 0 & 1 & 0 & 0 & 0 & -1 & 0 & 0 \end{bmatrix}
\begin{bmatrix}
dX(k) \\
dY(k) \\
dy(k) \\
S_R(k) \\
S_L(k) \\
dD(k) \\
df(k) \\
dB_s(k) \\
dB_{rb}(k)
\end{bmatrix}
+ v \qquad (14)
$$

where

$\hat{y}(k)$ - the calculated encoder heading angle,

$\hat{f}(k)$ - is a calculated heading angle using a gyroscope

v - measurement noise.

We assumed w and v to be white noise but we did not prove the accuracy of this assumption. The values for the covariance matrices were determined empirically and tuned through extensive tests. The technical specifications for the gyro were not particularly helpful in this regard. For instance, while the technical specifications provide rate errors, the Kalman filter required angle errors.

The followings are the assumed values for the system and measurement noises, respectively.

$Q = \text{diag}[(0.1m)^2, (0.1m)^2, (0.7°)^2, (0.00002)^2, (0.00002)^2, (0.00002)^2, (0.0001°)^2, (0.0001°)^2, (0.00003)^2]$

$R = (0.02°)^2$

4. EXPERIMENTAL RESULTS

In this section we present results from experime nts performed on a paved parking lot. The platform used in our experiments is the Pioneer AT four-wheel drive/skid-steer mobile robot shown in **Figure 4**.

The robot traveled along a pre-programmed, approximately square-shaped path, as also shown in Figure 5. The eight via-points that are marked by a '+' in Figure 5 were specified prior to the runs to define the path. The path planner then computed the angular and linear velocities to navigate the robot along the path. The robot traveled at a maximum speed of 1.5 m/s, but it reduced its speed to 0.8 m/s near the via-points in order to minimize deviations from the path. Figure 5 shows the trajectories of the robot. The robot traversed the 210-meters path in about three minutes and returned to the

Figure 4: The University of Michigan's Pioneer AT robot used in the experiments described here.

starting position. The odometry and gyroscope data were updated every 50 ms and 100 ms, respectively. Upon returning to the starting position, the difference, *D*, between the robot's actual position and the start position was measured with a measuring tape.

We performed experiments with and without gyro calibration and with and without Kalman filtering. In the experiments with the uncalibrated gyro the Kalman filter estimated the scale factor error. In the experiments with the calibration, the Kalman filter did not estimate the scale factor error but used the outputs of the calibrated gyroscope. In the experiments without Kalman filter, the orientation of the robot was only determined from the output of the gyro, and not from odometry.

We performed 10 individual, consecutive runs, five in clockwise (cw) and five in counter-clockwise (ccw) direction. The quantitative results of the experiments are summarized in Table II. The return position errors of Table II are the measured distance errors from the starting position (0, 0).

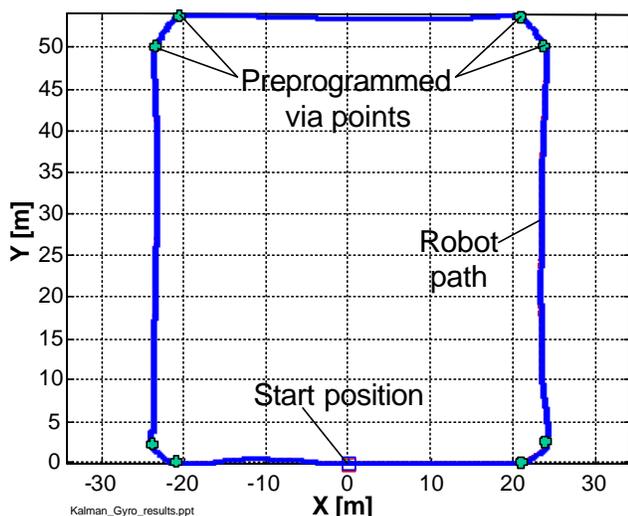As seen in Table II, when the measurements of the

Figure 5: Actual robot trajectory on the asphalted parking lot. In the experiment described here the robot performed five runs in clockwise (cw) and five runs in counter-clockwise (ccw) direction.

Table II: Return Position Errors after completing five runs in both cw and ccw direction along the square path of Figure 5.

	Without Calibration		With Calibration	
	Without Kalman	With Kalman	Without Kalman	With Kalman
a. Clockwise [cm]				
Run 1	94.4	27.3	8.9	5.3
Run 2	80.2	23.6	9.8	8.7
Run 3	75.8	17.7	15.8	10.9
Run 4	92.5	19.4	9.4	4.7
Run 5	72.3	19.3	25.9	17.8
Average	83.0	21.5	14.0	9.5
b. Counter-clockwise [cm]				
Run 6	124.4	56.2	24.9	19.3
Run 7	146.8	81.4	21.8	18.2
Run 8	133.8	70.8	20.1	14.8
Run 9	111.4	35.4	10.8	9.9
Run 10	145.4	80.3	15	12.7
Average	132.4	64.8	18.5	15

uncalibrated gyro were used, the performance of the positioning system is improved by using the Kalman filter since the Kalman filter compensates for the stochastic errors including the scale factor error of the gyroscope. However, when the measurements of the *calibrated* gyroscope were used, the improvement provided by the Kalman filter is relatively small compared to the improvement provided by our gyro calibration method. This is because our positioning system using only the calibrated gyro is very accurate by itself and the stochastic errors in the sensors are very small. Moreover, the effect of white noise of the gyro is not significant because it has a zero mean after compensating bias drift error. The characteristics of the state variances of the Kalman filter are as follows. The position and heading errors from the encoder and the gyroscope increase without bound because they are unobservable. However, the encoder scale factor error variances converge over time. The tread distance and gyro bias error diverge at a slow rate. Therefore, the filter can provide the robot with valid position and heading.

5. CONCLUSION

This paper presents two methods for improving the dead-reckoning accuracy of a mobile robot based on odometry and a fiber optic gyroscope.

The first method is a meticulous calibration procedure for fiber optic gyroscopes (FOGs). Our method compensates for 1) non-linearity in the scale factor, and 2) sensitivity to changes in temperature. We also employ a (trivial) method for compensating for the static bias drift. Our compensation method requires a series of test with the FOG mounted on a precisely controlled rotary table. Results from these runs are used to define a temperature-varying third-order polynomial calibration function.

The second method is the use of an indirect feedback Kalman filter. We developed a linear error state system model for implementing the indirect Kalman filter, in which the scale factor errors of the encoders, the distance error between the right and left wheels, and random bias and scale factor errors of the gyro were carefully modeled.

The experimental results from multiple 210-meter runs around a paved parking lot show that the gyro calibration is most efficient, resulting in a 7-fold accuracy improvement. The Kalman filter alone provides only a 2-fold accuracy improvement. However, when both methods are used concurrently, they provide the largest (9-fold) accuracy improvement. We conclude that a calibrated fiber optic gyroscope is the single, most effect sensor modality for mobile robot dead-reckoning systems. Although we did not explicitly test our calibration method with different FOG makes and models, we believe that the underlying error mechanisms are similar, and that therefore our calibration method can be applied to other FOGs as well. In that case, however, it may be necessary to change the order of the calibration function (in our case we found a 3rd order polynomial function to provide the best fit) according to the characteristic of each gyroscope.

6. REFERENCES

1. Bennett, S. M., Dyott, R., Allen, D., Brunner, J., Kidwell, R. and Miller, R., 1998, "Fiber Optic Rate Gyros as Replacements for Mechanical Gyros." *American Inst. of Aeronautics & Astronautics*, AIAA-98-4401, Boston, MA, Aug. 10-12, pp. 1315-1321.

2. KVH, 8412 W. 185th St., Tinley Park, IL 60477, USA, http://KVH.com.

3. Ojeda, L. Chung, H., and Borenstein, J., 2000, "Precision-calibration of Fiber-optics Gyroscopes for Mobile Robot Navigation." *Proc. of the 2000 IEEE Int. Conf. on Robotics and Automation*, San Francisco, CA, April 24-28, 2000, pp. 2064-2069.

4. Barshan, B., and Durrant-Whyte, H. F., 1995, "Inertial Navigation Systems for Mobile Robots." *IEEE Transaction on Robotics and Automation*, June, pp. 328-342.

5. Komoriya, K., and Oyama, E., 1994, "Position Estimation of a Mobile Robot Using Optical Fiber Gyroscope (OFG)." *1994 Int. Conf. on Intelligent Robots and Systems (IROS '94)*. Munich, Germany, Sept. 12-16, pp. 143-149.

6. Vaganay, J., Aldon, M. J., and Fourinier, A., 1993, "Mobile Robot Attitude Estimation by Fusion of Inertial Data." *Proc. of IEEE Int. Conf. on Robotics and Automation*, Atlanta, GA, May 2-7, pp. 277-282.

7. Park, K., Chung, H., and Lee, J., 1998, "Dead Reckoning Navigation for Autonomous Mobile Robots." *Proc .of Intelligent Autonomous Vehicle*, Madrid, Spain, March 25-28, pp. 775-781.

8. Press, W. H., Flannery, B. P., Teukolsky, S. A., and Vetterling, W. T. 1982, "*Numerical Recipes in FORTRAN: The Art of Scientific Computing*." 2nd ed. Cambridge, England: Cambridge Univ. Press, pp. 82-89.

9. Maybeck, P., 1979, *Stochastic models, estimation, and control Volume 1*, Academic Press, New York.

10. Borenstein, J. and Feng. L., 1996, "Measurement and Correction of Systematic Odometry Errors in Mobile Robots." *IEEE Transactions on Robotics and Automation*, Vol. 12, No. 6, December, pp. 869-880.